

RESEARCH

Open Access



Computational fluid dynamic simulation of packed bed drying process: impact of particle properties, drying conditions, and lateral edge heating modes on drying kinetics

Thi Thu Hang Tran¹ and Kieu Hiep Le^{1*}

Abstract

In this work, a two-dimensional computational fluid dynamic (CFD) model is developed to describe the drying process of a packed bed made of spherical particles. The volumetric evaporation rate inside the bed is computed from the pressure difference between the particle surface and the airflow. By using the thermal equilibrium assumption, the heat conservation equation is derived. The CFD model is solved in the COMSOL Multiphysics environment. The obtained results indicate remarkable maldistributions of temperature and moisture content. These maldistributions can be explained by the impact of lateral edges on thermo-hydraulic behavior. Additionally, the impact of particle diameter, air velocity, and bed width on the spatial-temporal moisture content and temperature distribution is investigated. It shows that the CFD model can be simplified to the receding front drying model for a bed made of small particles. Furthermore, by changing the thermal boundary conditions at the lateral edges, the influence of the heating mode at the lateral edges on the drying behavior is explored. The results indicate that contact heating at the bed wall can help to accelerate the drying process significantly.

Keywords Packed bed drying, CFD simulation, Contact heating, Particle diameter, Drying kinetic

1 Introduction

The particulate material can be encountered in both daily life and the industrial sector. To reduce the transportation weight and prolong the storage time, the water in the material should be removed. Several drying techniques such as fluidized bed drying, conveyor belt drying, pneumatic drying, spouted bed drying, and rotary drying have been widely applied to dehydration particulate material [1]. The advantage of these drying techniques is that the particles and grains can move forcibly, and the interaction between the drying agent and the drying

product is enhanced. However, these drying techniques become costly on both initial investment and operational costs for creating and maintaining the force moving and mixing of the material. Besides these mentioned drying techniques, the packed bed drying method where the air flows through a layer of immobile particles is known as the cheapest drying system. Additionally, it was proved that the particle moving can lead to mechanical damage, especially in the case of seed drying [2, 3]. To improve the efficiency of the packed bed drying systems, the fundamental understanding of the heat and mass transfer between the bed and the drying agent needs to be thoroughly investigated.

To describe the drying behavior of the packed bed, several heat and mass transfer models were developed. The simplest drying models are known as the empirical drying model such as the Page model, Newton model, and

*Correspondence:

Kieu Hiep Le
hieplekieu@hust.edu.vn

¹ School of Mechanical Engineering, Hanoi University of Science and Technology, Hanoi, Vietnam

Wang and Singh model [4, 5]. Since the parameters of the empirical models are fitted from experimental data, these models can well reflect the drying curve of the bed. However, the interpolation and extrapolation ability of the empirical models is questionable. The second group of the packed bed drying model is the one-dimensional continuum models which are developed based on the volume averaging technique [6–11]. However, the impact of the bed width on the drying behavior cannot be investigated by these one-dimensional drying models. This impact was investigated by using two-dimensional models [12, 13]. It can be seen that the lateral edges restrain the drying process due to the appearance of the hydraulic boundary layer. Recently, a CFD model was developed to express the drying process of a fixed bed in the work of Singhal et al. [14, 15]. This thin-layer CFD model extracts the void space from a random particle packing generated using the discrete element method simulation. Afterward, by performing the direct numerical simulation, the heat transfer coefficient can be obtained accurately, and a Nusselt number correlation can be estimated. However, due to its complications, this model is computationally expensive. Thus, it cannot be applied to depth packings where thousands of particles are considered simultaneously.

This work aims to develop a two-dimensional CFD model of packed bed drying which considers the coupling of the heat and mass transfer simultaneous interaction between the particle and the drying agent and of the interplay between drying agent flow and lateral edges. After the “1” section, the CFD model is briefly described. The CFD simulations are performed for a packed bed made of spherical wood particles. Besides the presentation of the temporal-spatial distributions of

moisture content and temperature inside the bed, sensitivity analyses are conducted to investigate the impact of particle diameter, bed width, air velocity, and heating mode at the bed wall on the drying behavior. Several remarks are drawn in the “4” section.

2 Model description

In this work, a packed bed of wet particulate material presented in Fig. 1 is considered. The hot air flows through the packed bed, and the thermal energy is transferred from the hot air to the bed for heating the bed and vaporizing the liquid water. The generated vapor diffuses to the drying agent, and it is released to the bed by the convective airflow. To develop the drying model, several assumptions need to be made

- The disorder of particle size is negligible compared to the size of the bed, and the thickness of the bed is relatively large compared to the particle size. For a bed with a random mono-modal particle assembly, a constant value of 0.4 of the porosity of the bed is used.
- The intra-particle distributions of moisture content and temperature are negligible. In other words, the particles are thermally thin.
- The hot air is slowly transported through the bed due to a high hydraulic resistance, and it has enough time to transport the thermal energy from the air to the solid phase. Thus, the temperature difference between the solid particles and airflow can be neglected and the local thermal equilibrium assumption for the solid and air can be hypothesized.

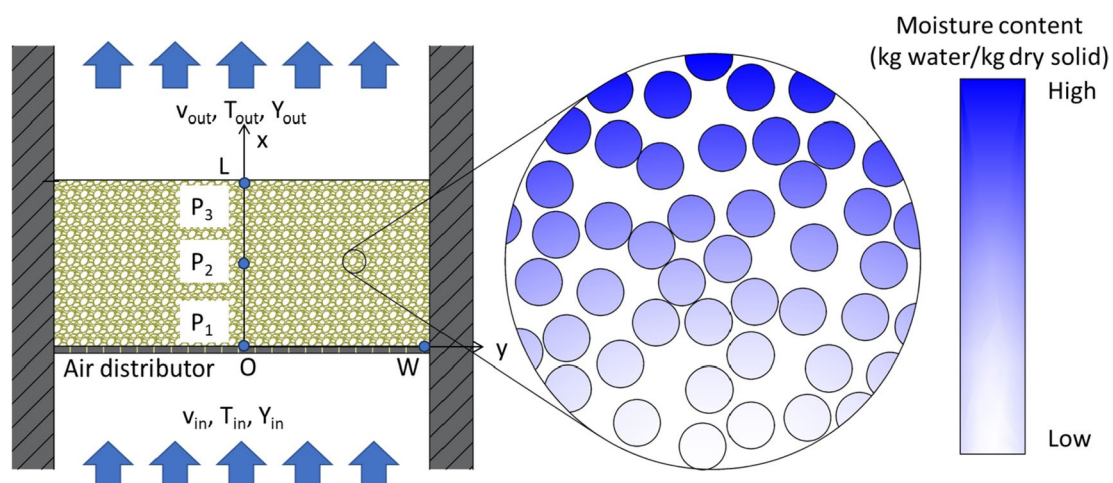


Fig. 1 Sketch of packed bed drying of the particulate material

2.1 Heat and mass conservation equations

The mass conservation equation of liquid water of the particles is derived as follows:

$$\frac{\partial}{\partial t}(\mathcal{E}_s \rho_0 X) + A_v \dot{m}_v = 0 \quad (1)$$

where $X = \frac{M_w}{M_s}$ (kg water/kg dry solid) is the moisture content of the solid, and ρ_0 (kg solid/m³) denotes the actual density of the solid particles. $\mathcal{E}_s = \frac{V_s}{V_g + V_s}$ is the volume fraction of the solid phase. As stated, for a randomly distributed packed bed, the constant solid volume fraction $\mathcal{E}_s = 0.6$ is used in the rest of this work. \dot{m}_v (kg water/m²/s) is the evaporation rate from the particle surface to the air:

$$\dot{m}_v = \beta \rho_a (Y_{\text{surf}} - Y_a) \quad (2)$$

In Eq. (2), ρ_a (kg dry air/m³) is the density of dry air, and Y_{surf} and Y_a (kg water vapor/kg dry air) denote the moisture content of air at the particle surface and in the flow, respectively. A_v is the specific volumetrical area (m²/m³) of the bed. For a bed made of spherical particles, the specific volumetrical area can be computed from the number of particles in a unit volume of bed as:

$$A_v = \left(\frac{\mathcal{E}_s \rho_0}{\pi \frac{1}{6} d_p^3 \rho_0} \right) \pi d_p^2 = \frac{6\mathcal{E}_s}{d_p} \quad (3)$$

The convective mass transfer coefficient β (m²/s) between particles in a packed bed and the airflow is computed from the Sherwood number by using the Ranz-Marshall correlation derived for a single particle as [16]:

$$Sh_{pb} = [1 + 1.5\mathcal{E}_s] \left(2 + 0.6\text{Re}^{0.5} \text{Sc}^{0.33} \right) \quad (4)$$

where $Sh = \frac{\beta d}{D_{\text{eff}}}$, $\text{Re} = \frac{\omega d_p}{\nu}$, and $\text{Sc} = \frac{\nu}{D_{\text{eff}}}$ are the Sherwood number, Reynold number, and Schmidt number, respectively.

The conservation equation of the vapor in the gas phase is derived as the change of the air moisture content is due to the convective air flow and the vapor source vaporized from the particles.

$$\frac{\partial}{\partial t} (Y_a \rho_a \mathcal{E}_g) + \nabla \cdot (Y_a \rho_a v_g) - \nabla \cdot \left(\rho_g D_{\text{eff}} \nabla \left(\frac{\rho_v}{\rho_g} \right) \right) - A_v \dot{m}_v = 0 \quad (5)$$

In Eq. (5), the velocity of hot air v_g (m/s) inside the bed is expressed by using the Darcy equation:

$$v_g = -\frac{K}{\mu_g} \nabla p_g \quad (6)$$

where K (m²) is the absolute permeability of the bed which can be computed by the Kozeny-Carman equation:

$$K = \frac{(1 - \mathcal{E}_s)^3 d_p^2}{180\mathcal{E}_s^2} \quad (7)$$

μ_g (Pa.s) is the dynamic viscosity of the gas. D_{eff} is the effective diffusivity of vapor in the air-vapor mixture. It can be expressed as a function of the bed porosity \mathcal{E}_g and of the binary diffusion coefficient of the vapor in air δ_{va} [17] as:

$$D_{\text{eff}} = \psi \delta_{va} \quad (8)$$

The energy conservation equation is written as:

$$\frac{\partial}{\partial t} (\rho_0 \mathcal{E}_s h_s + \rho_0 \mathcal{E}_s X h_l + \rho_v \mathcal{E}_g h_v + \rho_a \mathcal{E}_g h_a) + \nabla \cdot [(\rho_v h_v + \rho_a h_a) v_g] - \nabla \cdot [h_a \rho_g D_{\text{eff}} \nabla \left(\frac{\rho_a}{\rho_g} \right)] - \nabla \cdot [h_v \rho_g D_{\text{eff}} \nabla \left(\frac{\rho_v}{\rho_g} \right)] - \nabla \cdot [\lambda_{\text{eff}} \nabla (T)] = 0 \quad (9)$$

where h denotes the specific enthalpy of solid, liquid, water vapor, and air components. By using the constant specific heat capacity assumption, it can be computed as:

$$h_{s|l|a} - c_{p,s|l|a} (T - T_{\text{ref}}) \text{ and } h_v = c_{p,v} (T - T_{\text{ref}}) + \Delta h_{\text{evp}} \quad (10)$$

with the reference temperature $T_{\text{ref}} = 273.15$ K. Additionally, λ_{eff} is the effective thermal conductivity of the bed.

2.2 Initial and boundary conditions

In this work, a packed bed of spherical particles with a thickness of L is initially at a uniform temperature of T_0 and moisture content of X_0 . The drying agent with the temperature of T_{in} and moisture content of Y_{in} flows through the bed. The boundary conditions at the upper and lower edges of the bed are written as:

$$\text{At } x = 0 : T = T_0, Y = Y_{\text{in}}, v_x = v_{\text{in}} \quad (11)$$

$$\text{At } x = L : p = p_0, \frac{\partial T}{\partial x} = 0, \frac{\partial Y}{\partial x} = 0 \quad (12)$$

The left and right boundary conditions are expressed as:

$$\frac{\partial v}{\partial y} = 0, \frac{\partial Y}{\partial y} = 0, \frac{\partial T}{\partial y} = 0 \quad (13)$$

The proposed drying model is integrated into the CFD software COMSOL Multiphysics. The CFD simulations were conducted in a PC (CPU Core i7-9700 and 16 GB of RAM). The number of mesh was increased from 36,650 elements to 779,772 elements. The numerical moisture evolutions over time obtained with different meshes are presented in Fig. 2. As can be seen, the computational time strongly depends on the number of elements. However, when the number of elements exceeds 79,224 elements, the moisture content evolutions seem to be

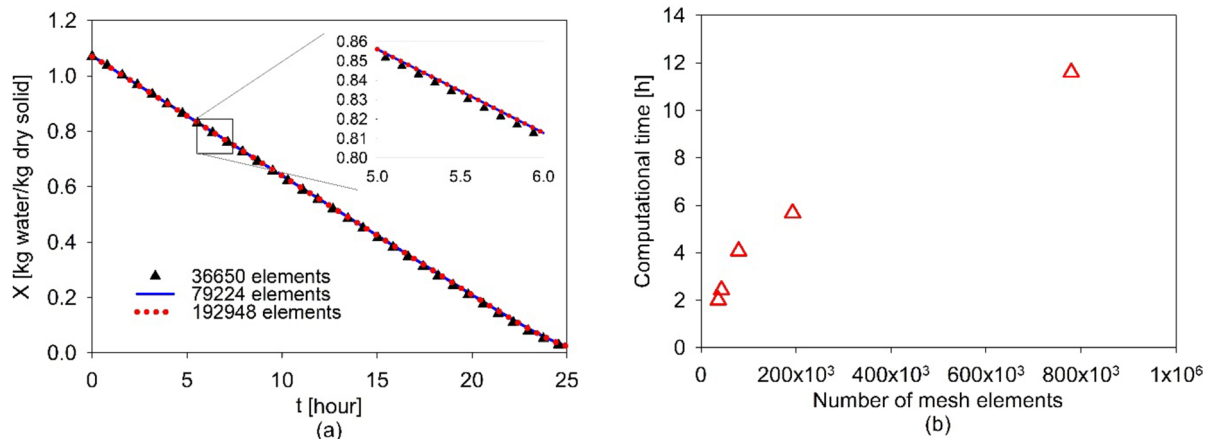


Fig. 2 The numerical moisture content evolutions over time (a) and computational time (b) obtained from different meshes

identical. Thus, the mesh of 79,224 elements was used in the rest of this work to avoid an expensive computational cost. With the mentioned PC and mesh properties, it took around 5 h for each simulation.

3 Results and discussion

The proposed model calculation is performed for a wood particle-packed bed with a thickness of 0.1 m and a width of 0.05 m. The geometrical and thermo-physical properties of wood particles are referred to from our previous work and listed in Table 1 [18, 19]. The simulation results are presented in Figs. 3, 4, 5 and 6.

As can be seen, the bed is not dried simultaneously. At the air inlet edge of the domain (refer to point P₁ in Fig. 1), the moisture content of wood particles drops

sharply. After 2 h, the wood particle at the air inlet edge is completely dried. However, the generated vapor at the air inlet edge led to an increase in the relative humidity of the drying agent (c.f. Figs. 4 and 5). The air at the outlet is almost saturated. Additionally, the temperature of the drying agent decreases due to the loss of thermal energy transferred to the wood particles. As a result, the moisture content of wood particles at points P₂ and P₃ (c.f. Fig. 1) starts to reduce very late after 5 and 15 h, respectively. The impact of the heat and mass impermeable boundary at lateral edges is demonstrated in Figs. 3, 4 and 5. The moisture content near the lateral edges is more difficult to remove compared to the center of the bed. The reason may come from the fact that the air velocity near the lateral edges is lower than the center. As a result, the convective mass transfer coefficient becomes smaller. The evaporation from the wood particle to the drying agent is restrained by a higher mass transfer resistance. Thus, convex upward contours can be seen in the moisture content, temperature, and relative humidity of air can be seen. To thoroughly investigate the influence of the lateral edges and other

Table 1 Thermo-physical properties of wood particles and the drying conditions used in simulations

Property	Value
Particle diameter d_p , mm	6.2 ± 0.3
Apparent solid density ρ_b , kg/m ³	743
Sorption isotherm $a_w = p_v/p_{v,sat}$	$a_w = \begin{cases} 1 & \text{with } X > X_{irr} \\ \frac{X}{X_{irr}} \left(2 - \frac{X}{X_{irr}} \right) & \text{with } X \leq X_{irr} \end{cases}$ $X_{irr} = 0.256 \text{ kg water/kg dry solid}$
Thermal conductivity λ_{eff} , W/mK	$\lambda_{eff} = 0.138 + \frac{X\rho_b}{\rho_l} \lambda_{eff}$
Specific heat capacity of dry solid $c_{p,s}$, J/kgK	770 ± 3.6
Initial moisture content of wood particles X_0 , kg water/kg dry solid	1.06
Initial temperature of bed T_0 , K	293.15
Inlet air superficial velocity v_{in} , m/s	0.05
Inlet air temperature T_{in} , K	333.15
Inlet air moisture content Y_{in} , kg vapor/kg dry air	17.85×10^{-3}

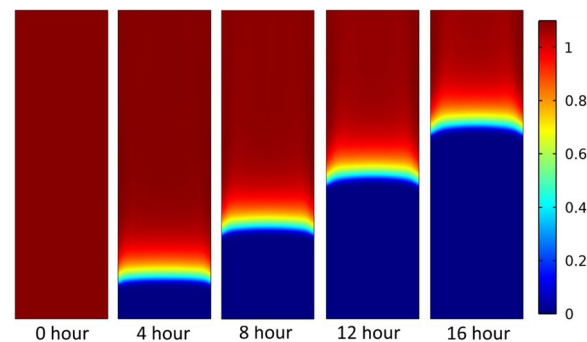


Fig. 3 Wood particle moisture content X (kg water/kg dry solid) distribution inside the bed sampled with a time interval of 4 h

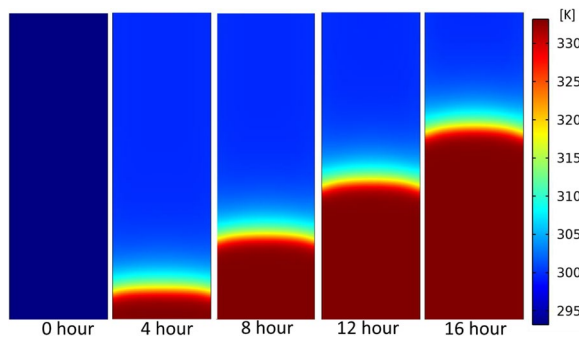


Fig. 4 Temperature distribution T (K) inside the bed sampled with a time interval of 4 h

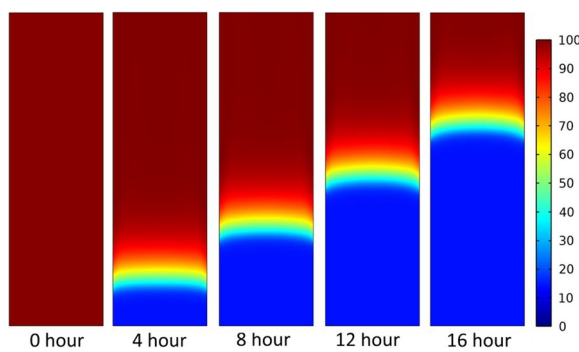


Fig. 5 Air relative humidity distribution inside the bed sampled with a time interval of 4 h

parameters such as particle diameter and air velocity on the drying process, a numerical sensitivity analysis is conducted. By performing simulations with the particle diameter varied in the range from 1.0 to 10 mm, the impact of particle diameter on the air pressure drop is presented in

Fig. 7. As can be seen, the pressure drop depends quadratically on the reciprocal of particle diameter. This behavior can be explained based on the Kozeny-Carman equation where the absolute permeability of the bed is proportional to the square of the diameter.

The influence of particle diameter on the drying kinetic is also investigated. The simulation results indicate that the impact of particle diameter on the evolution of the averaged moisture content of the bed is marginal. However, with the ascending of the particle diameter, both the specific volumetrical area of the bed and the convective mass transfer coefficient decrease. Thus, the drying time of particular particles becomes longer. This phenomenon can be seen in Fig. 8 where the moisture content evolution at the center point of the bed (referred to as point P_1 in Fig. 1) is presented. The moisture content of the particle with a diameter of 2.5 mm drops sharply whereas it reduces smoothly for the particle with a diameter of 10 mm. It means that for small particles, the receding front drying model where the bed comprised dried and wetted zones can be used to express the drying process of the packed bed. However, for large particles, the temporal-spatial heat and mass transfer model must be used to accurately simulate the dehydration process of a packed bed.

To pave the way for the design of a packed bed dryer, the influence of inlet air velocity on the heat and mass transfer in the bed is introduced in this paper. Instead of air inlet velocity varying from 0.05 to 0.4 m/s, the rest of the model parameters are kept as in Table 1. The feature results are presented in Fig. 9. Naturally, the higher inlet velocity results in a faster drying process. Thus, the moisture at the horizontal line with $x = L/2$ is almost removed after 150 min with an inlet air velocity of 0.4 m/s whereas

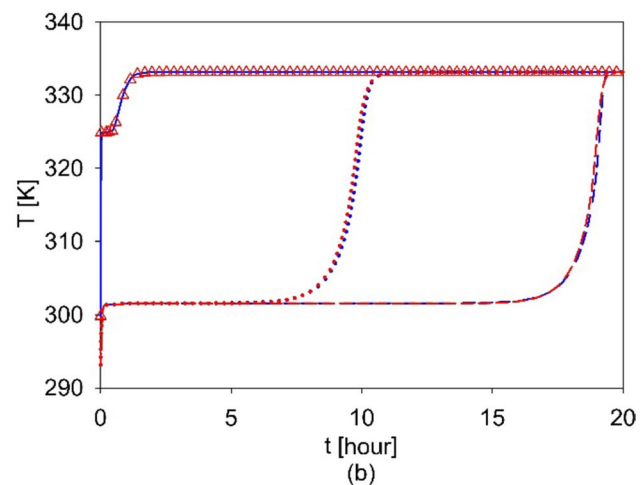
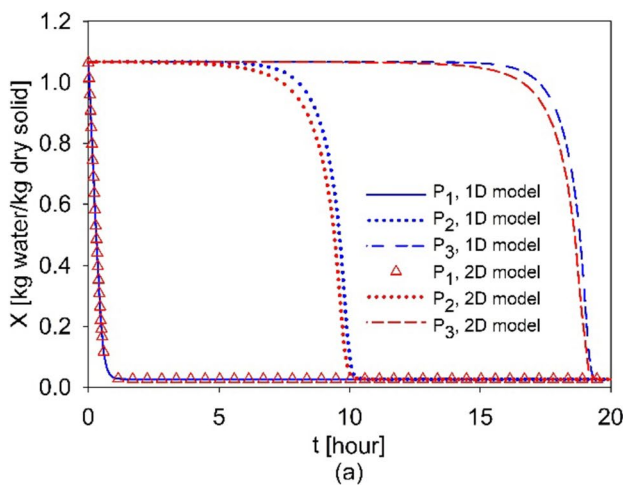


Fig. 6 Temporal moisture content (a) and temperature (b) evolution over time obtained at the inlet, the center and the outlet of the bed

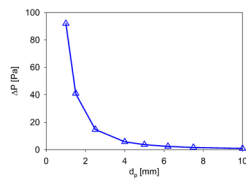


Fig. 7 Impact of particle diameter on the pressure drop of airflow through the packed bed

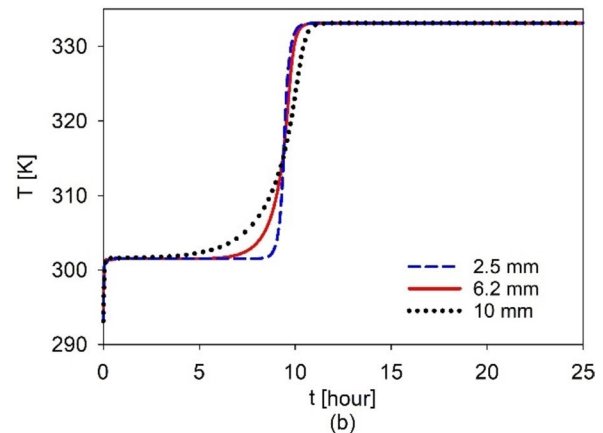
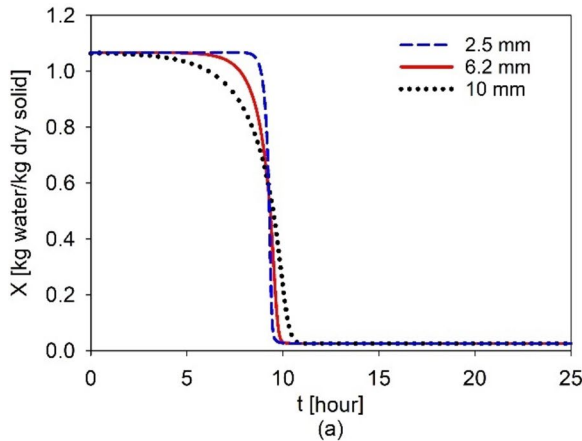


Fig. 8 Impact of particle diameter on the temporal evolution of moisture content (a) and temperature (b) at point P_2 (referred to Fig. 1)

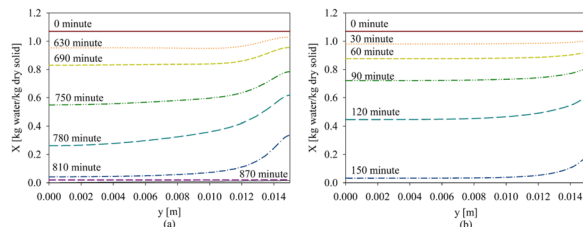


Fig. 9 The moisture content profiles at $x = L/2$ obtained with inlet air velocity of 0.05 m/s (a) and 0.4 m/s (b) at different times (referred to Fig. 1)

the water at this position needs more than 810 min to completely evaporate with an inlet air velocity of 0.05 m/s. Additionally, the results indicate that with small inlet velocity, the horizontal maldistribution of moisture content inside the bed becomes more significant indicated by a significant moisture content difference at $y = 0$ (at the center) and $y = W$ (at the wall).

Furthermore, the influence of bed width on the heat and mass transfer is investigated by varying W from 10 to 25 mm. The obtained results indicate that the drying time is not influenced significantly by the bed width. As shown in Fig. 10, the averaged moisture content and temperature at the horizontal line with $x = L/2$ obtained at

$t = 12.5$ h are identical. However, the moisture content and temperature profiles vary strongly with different bed widths. Near the bed wall, the slope of moisture content and temperature profiles become larger compared to the center of the bed. It implies that with a large width of the bed, the moisture content and temperature at the center of the bed are almost uniform. It means the influence of the lateral edges becomes more pronounced when the air velocity and the width of the bed are small.

For a further analysis of the impact of heat transfer at the lateral edges on the drying behavior, the CFD simulation was performed for constant temperature boundary conditions for the lateral edges: $T = T_{in}$. The simulation results are presented in Figs. 11 and 12. As can be seen, due to the heating effect of the lateral edges, the temperature near the edge increases quickly. As a result, the vapor pressure at the wood particle surface increases exponentially leading to the rising of the volumetrical evaporation rate (c.f. Eq. (2)). Hence, the moisture near the lateral edges is dried completely sooner compared to the center line. Thus, convex downward contours can be seen in the moisture content and temperature distributions.

4 Conclusion

In this work, a two-dimensional CFD model is developed to describe the drying process of a packed bed made of spherical wood particles. The mass interaction between the particles and airflow is described by using the sorption isotherm properties. By using the thermal equilibrium assumption, the heat conservation equation is derived for both wetted solid and fluid phases. The CFD model is solved in the COMSOL Multiphysics environment. The obtained numerical results show a convex contour in moisture content and temperature distribution.

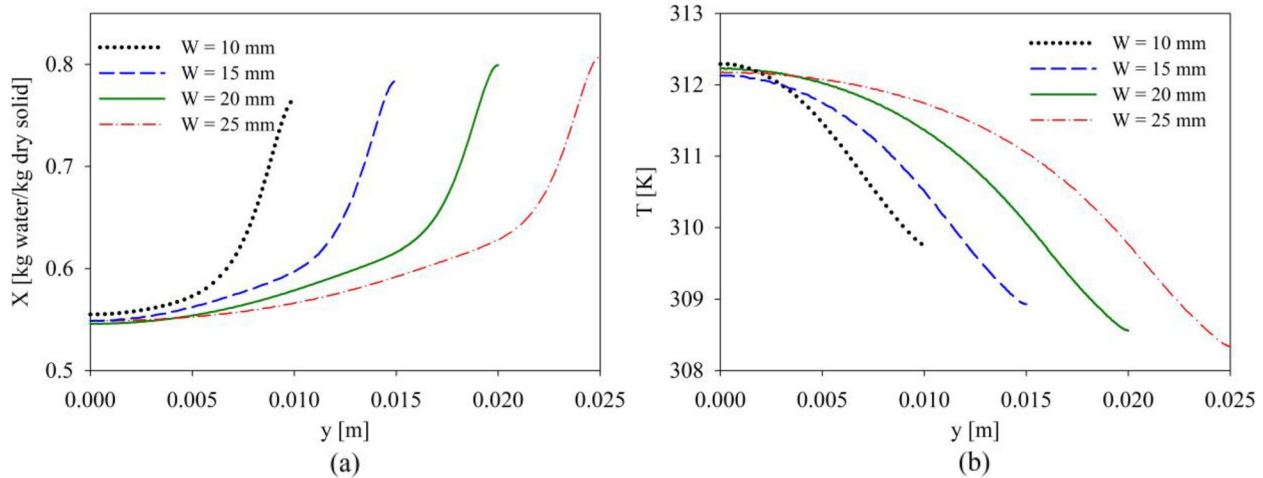


Fig. 10 The moisture content (a) and temperature (b) profiles at $x = L/2$ obtained with different bed widths (referred to Fig. 1) at $t = 12.5$ h

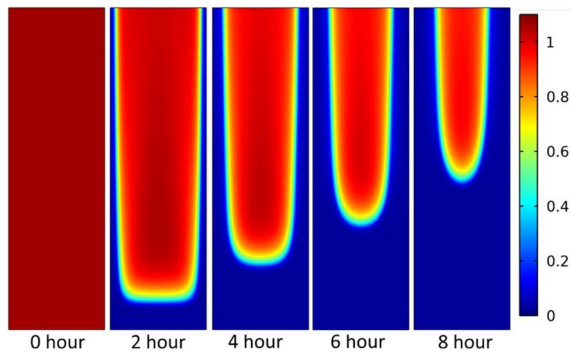


Fig. 11 Wood particle moisture content X (kg water/kg dry solid) distribution inside the bed sampled with a time interval of 2 h with contact heating boundary conditions

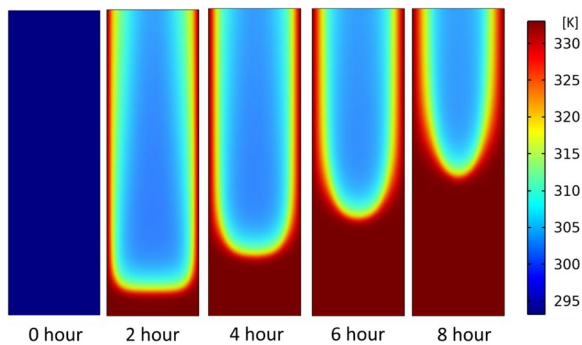


Fig. 12 Temperature distribution T (K) inside the bed sampled with a time interval of 2 h with contact heating boundary conditions

particle, the receding front drying model can be used to describe the drying process of the packed bed. The results also indicate that the impact of the bed wall on the heat and mass transfer becomes pronounced when the bed width and air velocity are small. The impact of the lateral bed wall on the drying process is remarkable when the bed is warmed up by both convective heat transfer from airflow and convective energy transport from the bed wall. In the future, the assumptions made during the development of the current CFD model shall be relaxed. For example, the thermal non-equilibrium phenomenon should be considered to model the intensive drying process conducted by the airflow with an elevated temperature and a high velocity. Additionally, the CFD results need to be validated against experimental observations. The experimental results can also contribute to the CFD model parameters to improve the simulation accuracy.

5 Nomenclature

- A Area, m^2
- A_v Specific volumetrical area, $m^2 m^{-3}$
- c_p Constant pressure specific heat capacity, $J kg^{-1} K^{-1}$
- d Particle diameter, m
- D_{eff} Diffusivity of vapor in air, m^2/s
- f Drying rate retardation coefficient, -
- h Enthalpy, $J kg^{-1}$
- Δh_{evp} Evaporation latent heat of water, $J kg^{-1}$
- K Absolute permeability, m^2
- L Bed thickness, m
- M Mass, kg
- \dot{m}_v Evaporation flux, $kg s^{-1} m^{-2}$
- p Pressure, Pa
- T Temperature, $^{\circ}C$
- t Time, s

It can be explained by the impact of lateral edges on the thermo-hydraulic behavior of the drying agent flow. Additionally, the impact of particle diameter on the temporal moisture content profile is investigated. For a small

V Volume, m^3
 v Velocity, $m\ s^{-1}$
 X Moisture content, kg water/kg dry solid
 Y_a Moisture content of air, kg vapor/kg dry air
 W Half-width of bed, m
Greek symbols
 α Heat transfer coefficient, $W\ m^{-2}\ K^{-1}$
 ϵ Volume fraction, -
 δ_{va} Binary diffusion coefficient of vapor in air
 λ Thermal conductivity, $W\ m^{-1}\ K^{-1}$
 ν Kinematic viscosity, $m^2\ s^{-1}$
 ρ_0 Mass density of dry sample, $kg\ m^{-3}$
 ρ_a Mass density of dry air, $kg\ dry\ air\ m^{-3}$
 ρ_v Mass density of vapor, $kg\ vapor\ m^{-3}$
Subscripts/superscripts
 eff Effective
 l Liquid
 in Inlet
 p Particle
 rad Radiation
 s Solid
 surf Surface
 sat Saturation
 v Vapor
 0 Initial value

Author contributions

Conceptualization, K.H.L.; methodology, K.H.L.; software, T.T.H.T.; formal analysis, T.T.H.T.; investigation, T.T.H.T.; data curation, T.T.H.T.; writing—original draft preparation, writing—review and editing, K.H.L.; visualization, K.H.L. and T.T.H.T.; funding acquisition, T.T.H.T. All authors have read and agreed to the published version of the manuscript.

Funding

This work was supported by funding from the Ministry of Education and Training (MOET), Vietnam (Grant number B2022-BKA-11).

Availability of data and materials

The data used to support the findings of this study are included in the article.

Declarations

Competing interests

The authors declare that they have no competing interests.

Received: 25 September 2023 Accepted: 11 January 2024

Published online: 26 January 2024

References

1. A. S. Mujumdar, *Handbook of industrial drying*, Advances in drying science and technology, CRC Press, Boca Raton 2014.
2. Barrozo, M. A. S., Mujumdar, A., & Freire, J. T. (2014). *Drying Technology*, 32(10), 1127–1141. <https://doi.org/10.1080/07373937.2014.915220>
3. Barrozo, M. A. S., Souza, A. M., Costa, S. M., & Murata, V. V. (2001). *Int J Food Sci Tech*, 36(4), 393–399. <https://doi.org/10.1046/j.1365-2621.2001.00470.x>
4. Jin, L., Li, Y., Lin, L., Zou, L., & Hu, H. (2015). *Fuel*, 152, 80–87. <https://doi.org/10.1016/j.fuel.2015.01.035>
5. Zanoelo, E. F., Di Celso, G. M., & Kaskantzis, G. (2007). *Biosystems engineering*, 96(4), 487–494. <https://doi.org/10.1016/j.biosystemseng.2006.12.006>
6. Bruch, C. (2003). *Fuel*, 82(6), 729–738. [https://doi.org/10.1016/S0016-2361\(02\)00296-X](https://doi.org/10.1016/S0016-2361(02)00296-X)
7. Stakić, M., Banjac, M., & Urošević, T. (2011). *Braz. J. Chem. Eng.*, 28(2), 273–384. <https://doi.org/10.1590/S0104-66322011000200012>
8. Peters, B., Schröder, E., Bruch, C., & Nussbaumer, T. (2002). *Biomass and bio-energy*, 23(4), 291–306. [https://doi.org/10.1016/S0961-9534\(02\)00052-1](https://doi.org/10.1016/S0961-9534(02)00052-1)
9. Prado, M. M., & Sartori, D. J. M. (2008). *Braz. J. Chem. Eng.*, 25(1), 39–50. <https://doi.org/10.1590/S0104-66322008000100006>
10. Ratti, C., & Mujumdar, A. S. (1995). *Journal of Food Engineering*, 26(3), 259–271. [https://doi.org/10.1016/0260-8774\(94\)00007-V](https://doi.org/10.1016/0260-8774(94)00007-V)
11. Wang, Z. H., & Chen, G. (1999). *Chemical Engineering Science*, 54(19), 4233–4243. [https://doi.org/10.1016/S0009-2509\(99\)00118-9](https://doi.org/10.1016/S0009-2509(99)00118-9)
12. Messai, S., El Ganaoui, M., Sghaier, J., Chrusciel, L., & Slimane, G. (2014). *Int. J. Simul. Multidisci. Des. Optim.*, 5, A14. <https://doi.org/10.1051/smdo/2013018>
13. Basirat-Tabrizi, H., Saffar-Avval, M., & Assarie, M. R. (2002). Proceedings of the Institution of Mechanical Engineers. Part A: *Journal of Power and Energy*, 216(2), 161–168. <https://doi.org/10.1243/09576500260049070>
14. Singhal, A., Cloete, S., Radl, S., Quinta-Ferreira, R., & Amini, S. (2017). *Chemical Engineering Science*, 172, 1–12. <https://doi.org/10.1016/j.ces.2017.06.003>
15. Singhal, A., Cloete, S., Radl, S., Quinta-Ferreira, R., & Amini, S. (2017). *Chemical Engineering Journal*, 314, 27–37. <https://doi.org/10.1016/j.cej.2016.12.124>
16. Gnielinski, V. (1980). *Chemie Ingenieur Technik*, 52(3), 228–236. <https://doi.org/10.1002/cite.330520306>
17. Vu, H. T., & Tsotsas, E. (2018). *International Journal of Chemical Engineering*, 2018(2), 1–13. <https://doi.org/10.1155/2018/9456418>
18. Kharaghani, A., Le, K. H., Tran, T. T. H., & Tsotsas, E. (2019). *Chemical Engineering Science*, 199, 602–612. <https://doi.org/10.1016/j.ces.2019.01.042>
19. Le, K. H., Hampel, N., Kharaghani, A., Bück, A., & Tsotsas, E. (2018). *Drying Technology*, 36(15), 1866–1881. <https://doi.org/10.1080/07373937.2018.1444633>

Publisher's Note

Springer Nature remains neutral with regard to jurisdictional claims in published maps and institutional affiliations.